METEOROLOGICAL APPLICATIONS
Meteorol. Appl. **18**: 372–382 (2011)
Published online in Wiley Online Library
(wileyonlinelibrary.com) DOI: 10.1002/met.244

RMetS
Royal Meteorological Society

Lidar observations of flow variability over complex terrain

A. Barkwith† and C. G. Collier*
School of Environmental and Life Sciences, Built and Human Environment Research Institute (BUHU), University of Salford, UK

ABSTRACT: This paper examines one way in which remote sensing instrumentation can be used to advance our understanding of the interactions between complex terrain and the atmospheric boundary layer (ABL). When mean flow speed is of moderate strength and the ABL is stable, mechanical effects will dominate thermal effects in modifying flow speed and direction. Boundary layer measurements were made using the scanning Salford 10 μm pulsed CO_2 Doppler lidar during the 2005 Convective Storm Initiation Project (CSIP), above the heterogeneous orography that surrounds Faccombe, Hampshire, UK. A new method of detecting boundary layer flow perturbations was developed and successfully applied to the lidar data, giving a clearer insight into flow modification that occurs above complex terrain. Copyright © 2011 Royal Meteorological Society

KEY WORDS lidar; heterogeneous; orography; atmospheric boundary layer

Received 12 July 2010; Revised 1 September 2010; Accepted 11 November 2010

1. Introduction

The effects of topography on air flow have many important implications. Areas of increased flow in the atmospheric boundary layer (ABL) (acronyms are also defined in Appendix) are beneficial when siting wind turbines or tall structures such as tower office blocks that may be adversely affected by strong winds. Boundary layer wind profiles also govern the amount of energy that may be usefully extracted from turbine systems. The dispersion of pollutant emissions are affected by flow variation generated over complex terrain. The spread of fire in forested areas is largely controlled by the flow of wind as it is perturbed by the rough forest canopy. At larger scales, the retardation of ABL flow as it crosses complex topography is a major input into climate and weather forecasting models.

The impact of non-uniform terrain on the ABL is difficult to predict, due to the turbulence produced by flow over and around the terrain involved and the complicated dynamic, fluid nature of the atmosphere. Whilst the ABL is driven by temperature and pressure differences that are relatively simple to simulate, it is also subject to frictional and Coriolis forces, stratification and buoyancy and density variations, which all make accurate simulation difficult. Over homogeneous terrain these additional effects are often relatively uniform.

Topography strongly controls the flux of momentum and energy between the terrain surface and the ABL. For example, in valley configurations the generation of flow perturbations arise from changes in roughness at the surface, slowing the mean flow (Wood and Mason, 1993). However, flow retardation can also come from the increased volume changes that lower elevation terrain exerts on the ABL. The slope angle of valley sides also affects ABL flow, with steep angles separating the adjacent flow from following the ground contours, causing increased turbulence. The *in situ* instruments previously used to measure ABL flow have a minimal spatial coverage, limiting their use in observing boundary layer flow perturbation. Alternative means of measuring the flow differences produced by topography is therefore needed.

Knowledge of flow over complex terrain has been gained through the use of wind tunnel and numerical experiments, and confirmed using field measurements. Progress was made in the understanding of ABL flow adjacent to hills by Jackson and Hunt (1975), who initiated the study of turbulent interaction of boundary layer flow and simple hill structures using linear analysis. Verification of the study has subsequently taken place during several field campaigns (e.g. Bradley, 1980; Walmsley *et al*., 1986; Coppin *et al*., 1994; Founda *et al*., 1997; Reid, 2003) and through laboratory study of flow using wind tunnel simulation (Finnigan *et al*., 1990).

Currently, flow prediction is dependent on numerical models that use complicated algorithms to simulate atmospheric dynamics. These models require huge computational resources and, consequently, can only be run on a limited number of computers worldwide. The spatial resolution at which these models process data is continually being refined, with global-scale numerical weather prediction (NWP) models using mesoscale dynamics, and flow prediction models used by the wind energy industry

* Correspondence to: C. G. Collier, National Centre for Atmospheric Sciences (NCAS), School of Earth and Environment, University of Leeds, LS2 9JT, UK. E-mail: c.g.collier@leeds.ac.uk
† Present address: British Geological Survey, Kingsley Dunham Centre, Keyworth, Nottingham, NG12 5GG, UK.

Figure 1. Outline of the UK, with exploded map of the area surrounding the lidar site and a 3D representation of the view looking southwest over the lidar (red dot).

at local scales (the latter of which are heavily constrained spatially).

Continuation of this refinement in the future will rely partly on improved knowledge of local scale flow differences, produced mechanically or by thermal processes. Currently, the most powerful operational NWP models have a resolution of 1 km, which does not capture all the effects of local surface-boundary layer interaction on their output (see for example Wyngaard, 2010). Large Eddy Simulation (LES) models may have resolutions of a 100 m or so, but require very significant computer resources to represent large volumes of the ABL, and complex parameterization schemes which may not fully represent ABL flow perturbations (see for example, Deardorff, 1970; Mason, 1994).

2. Doppler lidar measurements

The aim of the Convective Storm Initiation Project (CSIP) was to understand better where and how convective clouds form and develop into showers, and compare observations to numerical simulations using the fine-resolution Met. Office Unified Model (Browning *et al*., 2007). CSIP advanced the prediction of local distribution and timing of rain associated with deep convection by NWP models. Data on which this paper is based were collected during the 2005 field campaign of this project.

Faccombe (UK Ordnance Survey grid SU 390 581) is a hamlet situated about 15 km north of the Chilbolton Observatory, Hampshire, UK (Figure 1). The surrounding topography of fields and forest is contained within a few large estates. The area surrounding the Faccombe site is characterized by a mosaic of fields where areas of arable farmland are enclosed by hedgerows, and in some areas by mature trees. Parkland and some smaller fields with pasture are present. In some areas there is extensive and connected woodland cover, which occurs in association with valley sides. This produces a distinct landscape pattern comprising large, open, predominately arable fields on the higher areas, and long narrow areas clinging to valley slopes where woodland is intermixed with pasture. The lidar and other surface instrumentation were located 1 km north of Faccombe upon a ridge 5 km long (running approximately north–south), 1 km wide, and at a height of almost 100 m above the valley floors.

The different axes and scales of the major orographic features combined with the varying vegetation cover create a complex terrain for wind flow modelling. A simple breakdown of the area surrounding the Faccombe site allows it to be categorized into major surface type divisions, the largest (∼75%) of which is grazing and crop fields. There are small patches (making up ∼20%) of ash, maple and yew woodland and sporadic (total of ∼5%) farm buildings, hamlets and houses.

The Salford University lidar operated at 10 μm wavelength (Pearson and Collier, 1999). Atmospheric aerosol provided the targets from which lidar power in the beam was backscattered to the lidar detector. The motion of the aerosol provided estimates of wind speed towards or away from the lidar (see for example, Davies *et al*., 2001) Associated instrumentation was positioned about 1 km north of the hamlet at a height of ∼260 m above

sea level. The Faccombe site was chosen as it is elevated above the surrounding area. The field in which the lidar was sited is approximately 50 m^2 with a large wind turbine in the centre. The lidar, two Automatic Weather Stations (AWSs), and a radiometer were all positioned in the south west quadrant of the field where the lidar could produce scans uninterrupted by the wind turbine or the high hedges to the north and east of the field. Fencing, hedges and trees within the scanning area created 'hard' returns (only very slowly varying compared to aerosol backscatter) at elevations of 4° and below. Therefore, 5° was the lowest scanning angle performed for this project. The maximum elevation angle used was 20°, which produced a maximum distance to which the lidar can make measurements was approximately 3–4 km, dependent on the occurrence of cloud at the top of the ABL depth. The cell size of the lidar measurements, the range resolution, was 112 m.

The azimuth restriction placed on the lidar by the scanning mechanism allowed a maximum azimuthal scan of 295°. However, due to a malfunction of the computer driving the scanning mechanism at some points during the campaign this full range of movement was not always possible.

Other instruments at the Faccombe site used during CSIP were the Salford and Leeds AWSs, the tower mounted sonic anemometers, and the scanning microwave radiometer (see for example, Rose and Czekala, 2008), which is capable of retrieving vertical profiles of temperature and absolute humidity, liquid water path, integrated water vapour, and stability indices. The AWS retrieved surface temperature, humidity, wind speed, and direction. The sonic anemometers were mounted at 2 and 5 m, they recorded detailed three dimensional flow data. Radiosondes were released on specified Intense Observation Periods (IOP) days at regular intervals from the nearby Linkenholt and Larkhill sites, which are positioned at distances of 2.5 and 30 km, respectively, from the lidar location. Radiosonde observations were available on other days from the Larkhill site.

Measurements discussed in this paper were performed on seven days during July and August 2005 (see Table I). Higher angle (20°) scans were taken during CSIP IOP days while lower elevation (<15°) scans were taken on down days (non-IOP days). The elevation angle for IOP scans was determined by the requirements of the CSIP study. Further scans were taken, at fixed elevations, in increments of 2.5°, between 5° and 12.5°. The azimuth angle of the scans was chosen to retrieve data from as much of the ABL as possible. Although the maximum azimuthal coverage (295°) of the lidar was used whenever possible, scanner malfunction reduced the possible scan range of the lidar during a few measurements. The IOP scans took an average of 383 s to obtain (two elevation scans taken in a period of about 10 min), while the down day scans took an average 907 s, the difference being that more elevation angles were used for the non-IOP days.

Table I. Statistics for the high angle and low angle PPI scans.

	High angle scans	Low angle scans
Dates (dd/mm)	14/07 (Scan 141 approx one and a fraction scans between 12 : 31 and 12 : 41 UTC); 18/07; 26/07; 28/07	19/07 (Scan 192 between 1127 and 1142 UTC); 19 July; 09 August
Average scan time ± S.D. (s)	383 ± 110	907 ± 20
Elevation angle (°)	20	5, 7.5, 10, 12.5
Total number of scans	15	18

The scan numbers and times for two of the dates are shown in brackets.

The AWS, radiometer and sonic anemometers were run constantly throughout the 3 months of the CSIP campaign. Data from these instruments, combined with measurements gathered by regular nearby radiosonde releases, provided information about the state of the ABL not easily available from the lidar data. These data include, but are not limited to, temperature, humidity, water paths, stability and vertical velocity (no lidar vertical pointing was possible). It is important to know the stability of the ABL when analysing the data, as increasingly instability will mask the mechanical effects that topography has on boundary layer flow. Stability was derived from radiosonde measurements of temperature and potential temperature. The lidar data were split into two sections based on elevation angle high and low (as defined previously). The division was necessary as the information that can be derived from these different scan groups, and their level of validity, differ. A general description of CSIP instrumentation and a summary of ABL conditions for the CSIP area has been compiled by Leeds University (SEE, 2008).

A typical high angle Plan Position Indicator (PPI) plot, derived from scan 141, is given in Figure 2 with flow towards (red) and away from (blue) the lidar. It shows a southerly flow up to the top of the ABL, which in this case is approximately 1000 m. The noisy signal above this height is created by the reduction in aerosol content and resultant drop in signal to noise ratio (SNR). The noisy sector to the north of the scan was created by a hard object return close to the lidar; in this case it was from a tree. Velocity Azimuth Display (VAD) analysis (see for example, Browning and Wexler, 1968) of the PPI scan allows a profile of flow to be created for the ABL (Figure 3).

Low angled scans increase the volume of ABL that can be observed, as measurement is possible over greater distances. The high angle scans could measure a lateral distance of up to approximately 3000 m before the top of the ABL is reached, however, low angle scans were not limited by this factor and could record measurements of up to ranges approaching 8000 m. Figure 4 shows

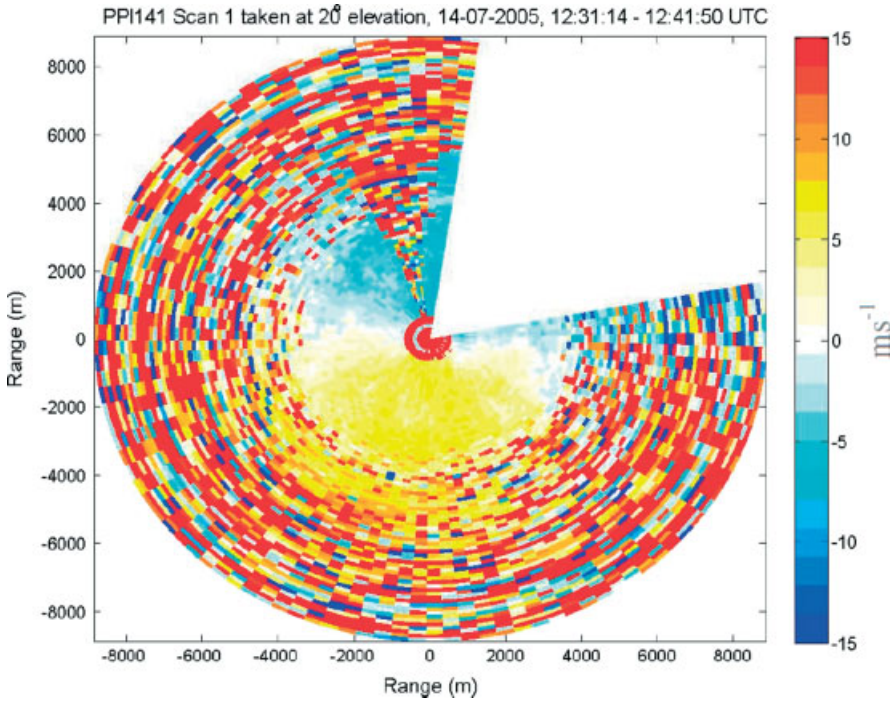

Figure 2. Typical high level PPI scan 141 taken at 20° elevation at 123 114 UTC 14 July 2005. ABL height is indicated by the increased speckling.

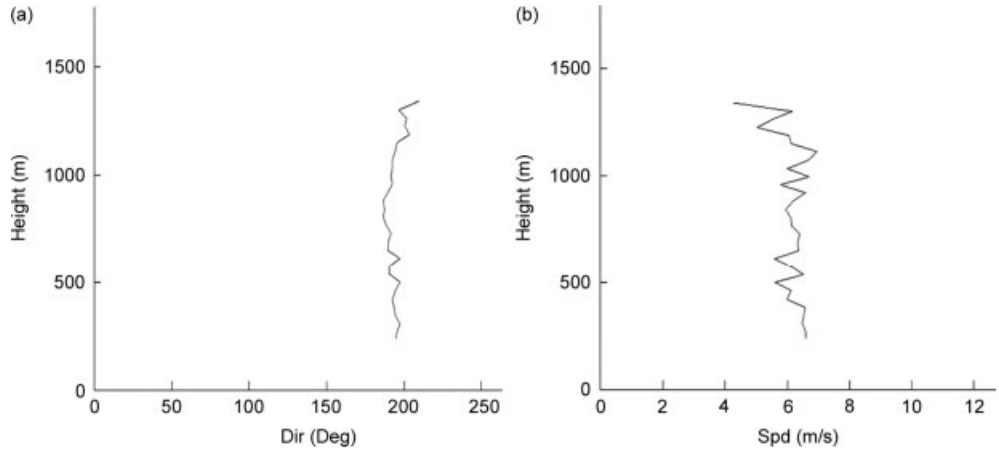

Figure 3. VAD analysis of PPI scan 141 1231 UTC 14 July 2005 giving the horizontal wind direction and speed up through the ABL.

the typical distances reached by the lidar at different elevation angles before the top of the ABL is reached, which in this example is assumed to be 1200 m.

The PPI plot derived from a low angle scan 192 (Figure 5) was taken at 7.5° elevation. Unlike high angled scans, measurement distance in this case is limited to 8000 m by the lidar optics rather than the ABL depth. Over half of the scan is within 500 m above the heterogeneous terrain, enabling the associated turbulent structures to be more readily identified and increasing the possibility of locating a specific source. Scan 192 reveals a westerly wind with little variation in direction up through the ABL and speed increasing from 9 m s^{-1} at ground level up to 12 m s^{-1} at the maximum scan height, represented by the stronger colours at the outer boundary. VAD confirms the PPI analysis for this scan, however, turbulent structures remain difficult to identify from either the PPI or VAD output.

3. Lidar wind field analysis

The initial challenge in the analysis of lidar wind fields was to create a means of displaying flow heterogeneity. The need to make the display accurate and flow disturbances easily identifiable meant that the lidar data had to be post-processed. The display used is based upon the PPI plot technique commonly used to display radial flow patterns, as they have the potential to convey all the required information. The lidar-derived vertical profile of the horizontal wind velocity was used as input to a numerical model described in the following paragraphs, from which

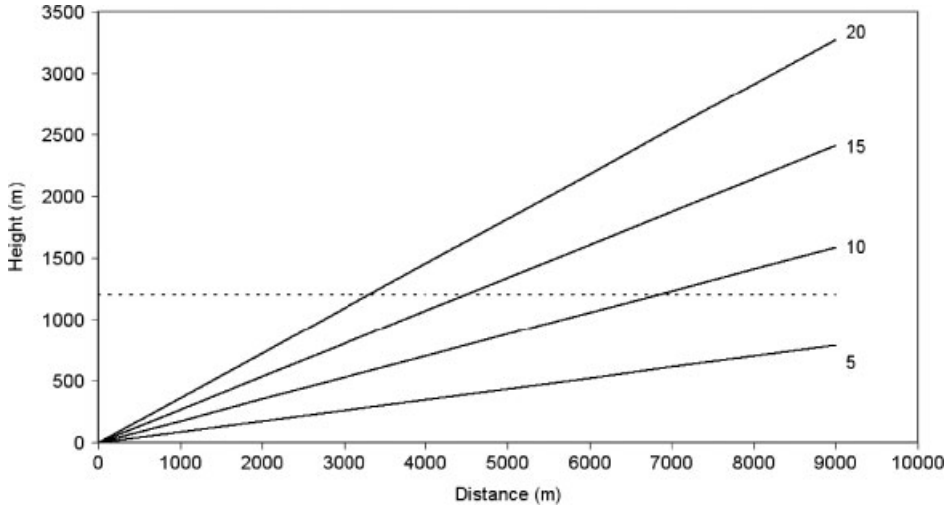

Figure 4. Differing lidar beam elevation angles (5°, 10°, 15°, 20°) penetrating the ABL top at height of 1200 m above lidar.

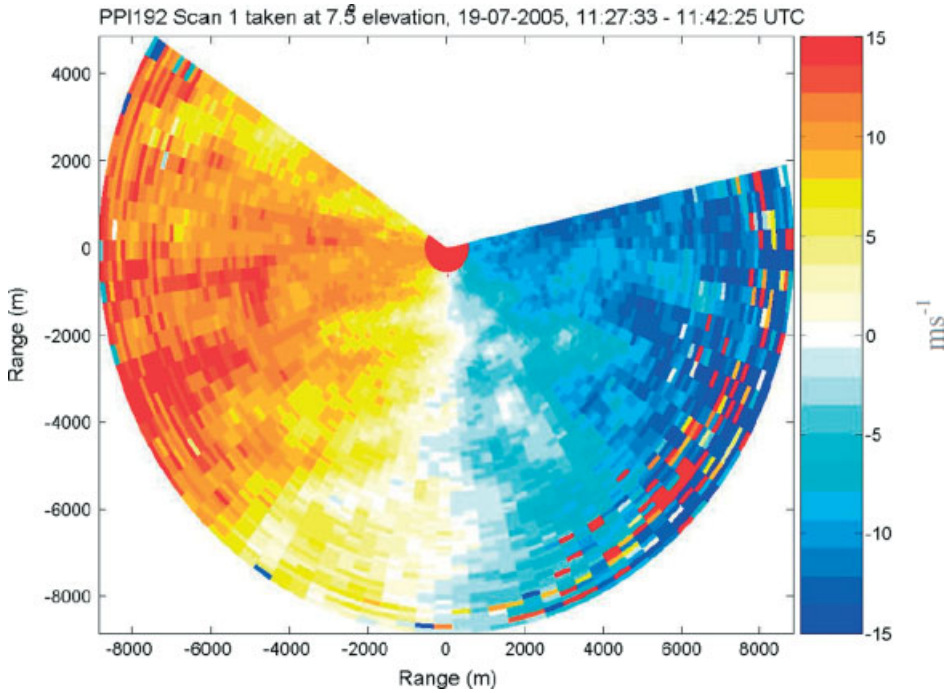

Figure 5. Typical low level PPI scan 192 taken at 7.5° elevation, 112 733 UTC, 19 July 2005.

a reference PPI plot for linear (no turbulence or spatial variability) ABL flow was produced. Such plots are known as the difference model lidar (DML). The spatial and temporal accuracy of the input lidar data are retained through the post-processing.

The DML program was written in M-code, designed for the MATLAB (matrix laboratory) desktop software package. MATLAB is a numerical computing environment that combines algorithm implementation with a simple user interface. MATLAB's availability and ease of use make it the ideal environment in which to create numerical models. It can interface with other programs and in other languages (C and FORTRAN), allowing direct data input from a number of sources. The model is based on the work of Wood and Brown (1986), shortened to WB-86 for the remainder of this paper. Although WB-86 determined wind field properties using Doppler radar, the same principles can be applied to the Salford Doppler lidar. WB-86 derived the equations needed to calculate a mean flow profile from a PPI styled plot. The reverse of this procedure was used to create a PPI style plot from a VAD derived ABL flow profile. The plot produced is free from the effects of local heterogeneity and was compared to measured data.

A Cartesian coordinate system was used with x positive towards the east, y positive towards the north and z positive upwards. The centre of the coordinate system is the lidar location. The lidar beam is directed at an elevation angle (α) and rotated around the vertical axis at an azimuth angle (β) to the x axis. The horizontal range (r)

of a particular range gate (R) at a distance, R_d, is given as:

$$r = R_d \cos \alpha \quad (1)$$

The azimuth variation in mean velocity V_R for a range gate is calculated using the x and y velocities (V_x and V_y respectively):

$$V_R = V_x(\beta) \cos \beta \cos \alpha - V_y(\beta) \sin \beta \cos \alpha \quad (2)$$

The known variation in velocity for R at differing α and β are combined to produce a VAD derived mean velocity profile of the ABL, allowing the production of PPIs for idealized situations or for real data. At higher elevations Equation (2) should include a component of the vertical wind velocity. This is assumed to be zero in this analysis, an approximation which is only likely to be weak at elevations above 20°.

During the early testing stages the model was initialized using simplified representations of ABL flow profiles with fixed u, v, and z with height. This allowed the modelled output PPI (MPPI) to be directly compared with the work of WB-86, who themselves produced PPI plots from simplified ABL equations. It should be noted that work published by WB-86 is independent of flow speed: the only constraint on speed is the amount of variation through the ABL profile. However, for a quantitative study of ABL flow heterogeneity a known flow speed is essential. Therefore, speed has been included in this work from the basic equations through to the full model. When compared with the work of WB-86, an arbitrary flow speed was used in the equations. This does not affect the pattern of the MPPI, only the range of flow speed, allowing a direct comparison with published results by WB-86. The level of elevation used is the same as that of WB-86 for each scan.

The modelled output was compared with all WB-86's published PPIs produced from idealized ABL profile equations. The published equations range in complexity from simple fixed u with increasing height to examples more representative of the ABL, for example non-uniform directional and speed shear. All were found to be a good match in terms of the PPI patterns produced, which are speed independent.

After the idealized input testing phase, the MPPI program was modified to allow input from data collected during the field campaign. It could then be initialized from a variety of different remote sensing devices which provide vertical profiles of ABL wind velocity.

A program was created to perform VAD analysis on each range gate height within a lidar PPI scan. The mean flow speed and direction were recorded for each gate height and combined, producing a file containing a vertical profile of ABL wind velocity for each scan processed. For each PPI scan in this study, the lidar made three sweeps along the azimuth and temporally averaged the data for each range gate. The spread of observations for each gate increases with ABL height, due to increases in measurement error introduced by an elevation in SNR further along the lidar beam. With a profile of ABL flow for a particular PPI, the program could be initiated.

The final step in the MPPI is the derivation of the vertical profile of the horizontal wind velocity, averaged for each range gate height, with no external influences. The MPPI can be directly compared with the PPI from which it was created and quantitative differences can be highlighted.

Unlike PPIs, the MPPIs have no locally produced flow perturbations within their output. Therefore, to disentangle and highlight the effect of local heterogeneity on flow, the MPPI (linear flow) needs to be subtracted from the PPI (linear, spatial variability, and turbulent flow), leaving just the flow perturbation characteristics. The resultant plot of the output containing the turbulent characteristics was named the DML (Difference Model Lidar plot).

DML plots were created for each of the CSIP PPI scans in order to ascertain the local topographical effects on ABL flow. The following sections of this paper give the derived DML plots, possible links to local topographic features, comparison to other data, and assumptions that have been made.

4. DML comparisons

The high angled PPIs share the feature of speckling around the fringes of the scan where the top of the ABL is penetrated, and SNR is reduced. Figure 6 shows the DML plot for scan 141, where areas of increased and decreased flow can be seen within the central area. Differences of up to ± 3 m s^{-1} are apparent throughout the plot (the outer area of noise can be ignored), which is expected due to the complex topographic nature of the site.

The variations in flow are not randomly arranged within DML 141, where they form distinct areas of flow deviation which measure 300–1500 m in diameter, with greatest deviation at the centre of each. Structures of this size are expected to relate to the nature of the underlying orography and larger surface roughness elements. It is, however, difficult to study the lateral extent of the turbulent features seen in DML 141 and the other high angle scans, due to the lateral spatial limitation placed on the results by the elevation angle (20°). These limitations are not present in the lower angle scans.

The high angle plots do not clearly indicate the lateral extent of the turbulent features, whereas the low angle scans do convey this information more clearly. There are distinct structures composed of increased or decreased flow speeds that are again comparable in scale to local topographic features (e.g. hills, valleys, forests and urban areas). The largest flow structures, defined laterally, extend up to 4000 m in length and are 500 m wide. There are numerous smaller structures present, the smallest being 300 m in length and breadth. Variations in flow speed in DML 192 are greater than those in DML 141, regularly exceeding ± 3 m s^{-1}. This increase is due to the increased wind speeds present, and not representative

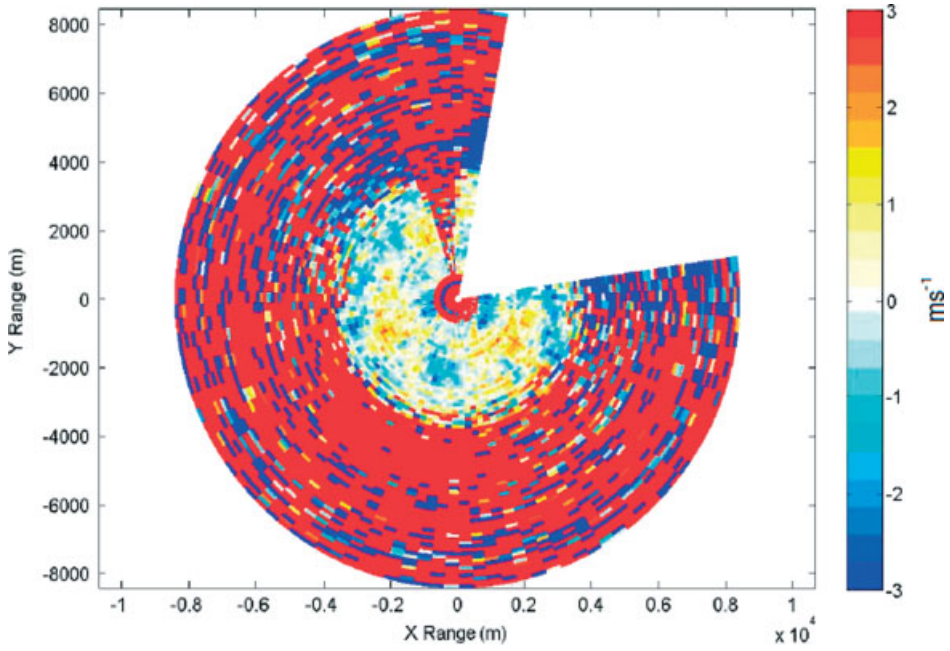

Figure 6. DML plot for scan 141. Heterogeneous flow features are represented by their deviation from an average.

of all the lower angled DML plots. Differences in turbulent structure location will vary with flow speed, flow direction, and elevation angle. The DML plot derived from PPI 191 was scanned at an elevation angle of 10°. While many turbulent structures are present, they vary in location and strength when compared to DML 192 and the other DML plots. However, the size and position of these structures remains approximately the same in all scans taken on days with similar atmospheric conditions with regards to neutral stability and sufficient but not excessive flow speed.

Identification of the possible source areas for the turbulent structures within the DML plots is now attempted. This is necessary as the turbulent ABL structures produced by flow-surface interactions do not occur directly above the surface feature, but downwind. DML data from 19 July 2005 is used as an example due to its well defined turbulent features, the lateral extent of the scans, the range of scan angles, and the ABL conditions present when the data was collected.

There are two ways to solve upwind fetch: these are based on Lagrangian trajectory models or analytical solutions of the advection-diffusion equation in an Eulerian reference frame (see for example, Schmid, 1994). Both assume flow conditions that are not disturbed by obstacles or topography, negating their use in this study. Therefore, a qualitative approach was applied in order to identify the source areas of flow perturbation. An orographic map of the area covered by the lidar was sectioned into areas that, based on the literature noted in Section 1 of this paper, would be expected to either increase or retard flow speeds (Figure 7). For this diagram an average terrain height of 187 m (black solid line) was calculated, and anything above 200 m was marked as a possible source for increasing flow speed. The orography between these heights is considered to be neutral. Areas below 175 m were marked as areas likely to lower flow speeds. The red dot in Figure 7 indicates the lidar location and the black rings represent lidar ranges of 3000, 6000, and 9000 m. The smaller the roughness length of an object, the less the vertical range of its ABL flow disturbance. It is expected, therefore, that turbulent structures towards the fringes of the scans are more likely to have an orographic source (roughness length, $z_0 > 2$) rather than an urban ($z_0 < 0.5$) or vegetation source ($z_0 < 0.2$). The diagrams are skewed towards the south west, allowing the orography of the flow source to be taken into account.

With the base map complete, the DML plots can now be overlaid in a DML overlay (DO) plot. Figure 8 is an example of a DO for DML 192 draped over the base map. It has had the neutral 'differences' removed, allowing more of the base map to be seen. The 187 m contour remains overlaid as a means of identifying potential

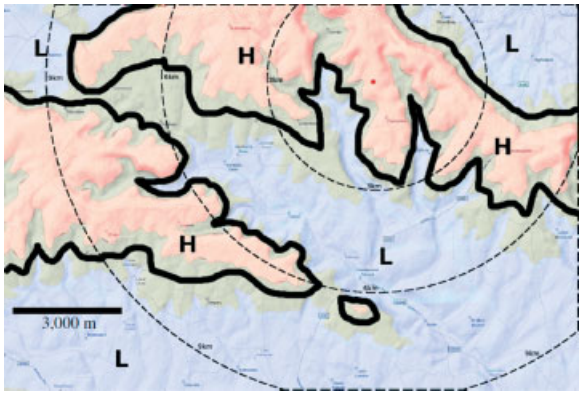

Figure 7. Map of potential flow disturbance sources for the Faccombe area. Red indicates increases in speed due to orographic changes (designated by the letter H) and blue representing decreases (designated by the letter L). Areas between are considered neutral.

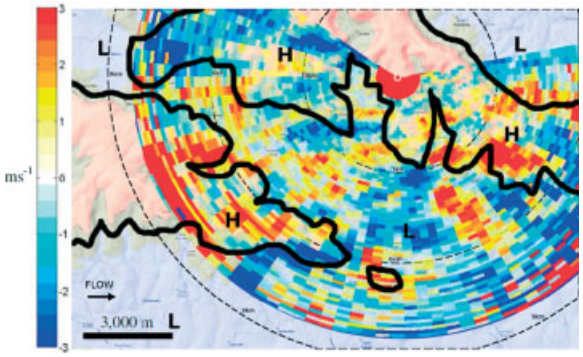

Figure 8. DML 192 draped over a base map. Neutral areas of the DML have been removed.

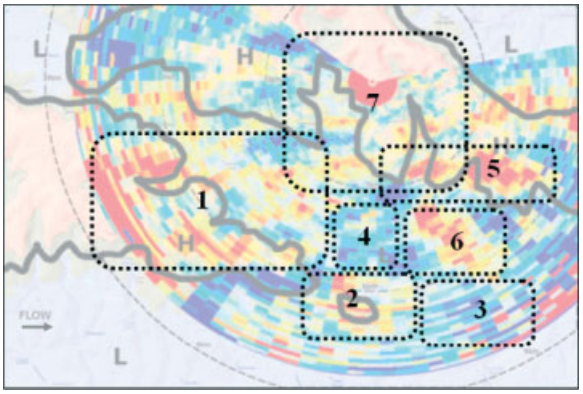

Figure 9. Selected areas for qualitative analysis into apparent flow structures.

orographic sources. The mean flow direction, derived from VAD analysis of PPI 192, has been included in the lower left hand corner. Knowing the flow direction is important when interpreting the data as the direction of potential sources will be apparent. There appears to be a good level of correlation between elevated terrain and higher flow speeds downwind of a potential orographic source of flow variation. The largest flow disturbances will now be discussed with respect to possible orographic sources. Figure 9 highlights the areas to be analysed.

Area 1 (A1) shows a well defined block of highly elevated wind speeds (up to $+5.4$ m s^{-1}) in the west, fading to patchy elevated flow speeds in the east (up to $+2.8$ m s^{-1}). The underlying orography includes a transition of ridge to valley from west to east. With the westerly wind direction it is expected that the resultant increase in flow created by the ridge should be detected above the valley area. A2 is an example of increased flow speeds over a hill of up to $+3.7$ m s^{-1}. Care must be taken when interpreting the causes of flow disturbance as the PPIs increase in height from the lidar site. In the case of A2 it is more likely that the increase is related to the ridge to the west of the area. A3 and A4 are both located over the central parts of valley areas, exhibiting reduced flow speed (-3.0 and -3.4 m s^{-1} respectively). Within A5 there are two areas distinguishable by their highly increased flow speeds with smaller increases between. Below and to the west of each of these the terrain forms a ridge formation followed by a valley. This type of terrain transformation is a good candidate for the source of the flow disturbances in A5.

For DML 192, A7 has a minimum measurement height of 150 m and a maximum of 400 m (above the lidar site), this is the most likely area where we could see the affect of smaller roughness features on the ABL, as measurements are closest to the surface. This area has been expanded in Figure 10, and the previous base map (Figure 7) has been modified to include areas of increased roughness (green), such as forest, that are thought to have an effect on ABL flow. The resulting diagram (Figure 11) has been used to compare areas of enhanced smaller scale ($z_o < 0.3$) roughness with measured low level (<400 m) flow anomalies. DMLs for all the dates and angles have been analysed in a similar manner. The results shown from DML 192 are representative of all measurements in terms of the persistence and location of the features from one scan to another taken under the favourable ABL conditions described previously.

Unlike the comparison of DML with larger scale orography, the comparison of DML to smaller scale roughness does not have any inherent connection. Although well defined areas of flow disturbance do exist in the scan at these lower measurement heights, they are not directly linked to the smaller roughness scales. This result was found in all of the DML plots from the CSIP campaign.

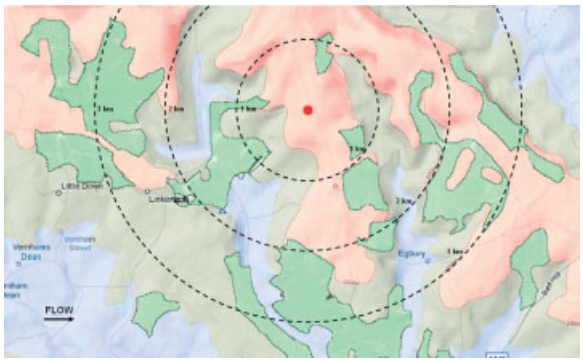

Figure 10. Orographic flow disturbance sources for the Faccombe area with areas of major surface roughness, such as forests and urban areas, overlain.

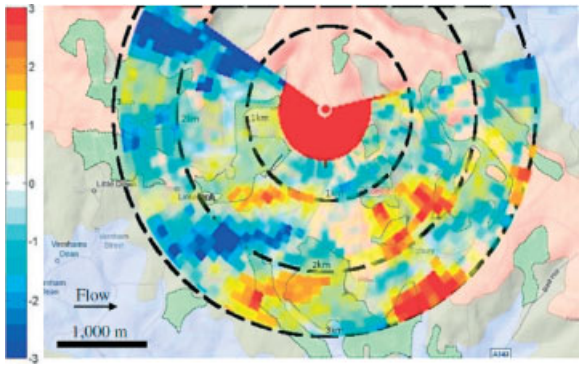

Figure 11. Differences in enhanced smaller scale roughness (shown green) with measured low level flow anomalies from DML 192.

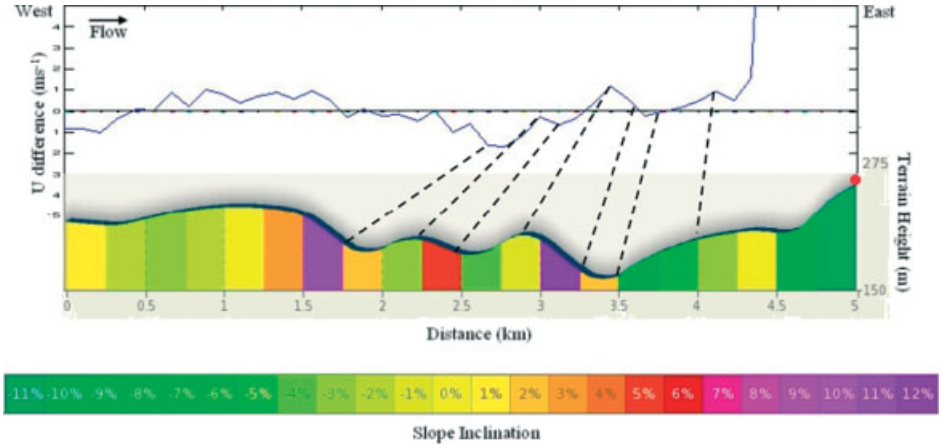

Figure 12. CSD (192 west) with links between terrain and DML differences shown.

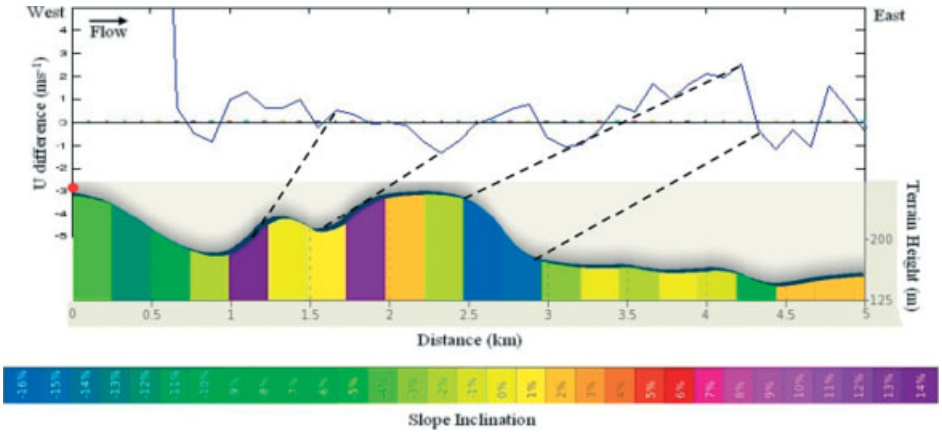

Figure 13. CSD (192 east) with links between terrain and DML differences shown.

Quantitative, and further qualitative, links between orography and the turbulent structures were found by looking at the flow differences along the mean flow direction, referred to as a cross section DML (CSD). The one dimensional nature of the data allows results to be compared to a cross section of orography. To ease comparisons, the cross sections were divided into 250 m sections and the inclination for each calculated as a percentage. The lidar location is given by the red spot, with flow indicated as a black arrow. There is vertical exaggeration within the cross sections, enabling easy identification of orographic features. The highest and lowest flow speeds and directions recorded by the lidar were also processed for PPI 192, allowing maximum and minimum measured perturbations to be included on CSD 192.

The most prevalent orographic features were selected on the CSD plots and linked to the ABL disturbance most likely to have been created by that feature. This allows the ABL flow difference for each terrain element to be analysed quantitatively, allowing comparison with a Numerical Weather Prediction (NWP) data set which will be the subject of a future paper. Figures 12 and 13 include these linkage lines for CSD 192, which have had beam height, flow direction, and flow speed taken into consideration when being plotted. The difference in inclination of each link is related to measurement height, with the highest disturbances occurring the furthest (laterally) from their source.

5. Discussion

The difference in height from the average (187 m) of each section was plotted against the difference in flow speed for each CSD plot. Figure 14 is the resultant graph for CSD 192 (east and west). This process was repeated for each CSD from 19 July and a linear regression was performed on the data, giving a combined R-squared value of 0.31. This indicates a link between terrain heterogeneity and the ABL flow differences observed in the DML plots.

Table II shows the R-squared results of linear regression for CSD 192, the CSDs for the 19 July data, and for the entire range of scans. Such low linear regression results make the individual data sets statistically insignificant; however, it does allow the data sets to be quantitatively compared with each other. The less stable days show less correlation between topography and ABL flow differences. This is to be expected, as an increase in thermally generated turbulence occurs during periods of ABL instability. The methods described do not account

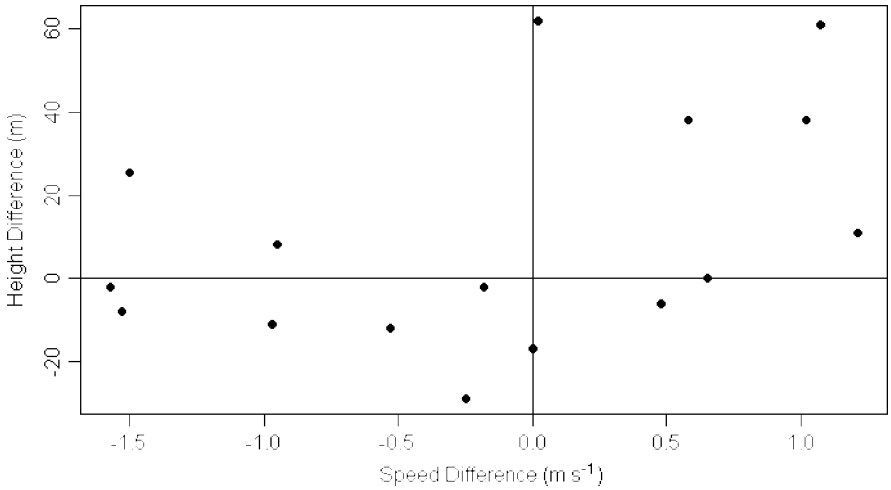

Figure 14. Graph of the difference in terrain height from the average, (187 m) against observed difference in flow speed.

Table II. Derived R^2 value from linear regression performed on different CSD data sets.

CSD data set	R^2	Number of samples
CSD 192	0.22	16
19 July	0.31	208
Stable/neutral days	0.29	448
Unstable days	0.09	160
All days	0.17	608

for influences on ABL flow from outside the observation range of the lidar. It is assumed to be flat and at a height equal to the terrain height average (187 m). This is of course not the case, but the assumption is necessary to limit the study to a manageable size. In addition to this, the CSD results are taken along mean wind direction, any deviations in flow the mean will produce lowered R-squared values as orography outside the cross section is ignored.

Using the CSD data from the stable/neutral days a relationship between terrain height difference (h_d), and flow speed difference (Δu) was formulated:

$$\Delta u = \frac{h_\mathrm{d} - 7.94}{17.08} \tag{3}$$

This result is a little different than expected. It implies that at the neutral terrain height ($h = 187$ m and $h_\mathrm{d} = 0$) where flow difference is expected to be zero, a negative flow speed of $\Delta u = -0.46$ m s^{-1} is calculated. There are several explanations for this including: non-mechanical generated flow perturbations; external orography affecting flow from outside the narrow band of terrain covered by the one dimensional sections; and the terrain height being above average along the CSD scans. Each of these explanations is discussed further in Barkwith (2009). Once the topographic source for a particular turbulent structure has been identified, through either of the methods described above, a qualitative assessment of the level to which the ABL is perturbed may be carried out and contrasted with the model. The method of using CSD to obtain results is perhaps the simplest, as the amount of data contained, and its subsequent processing, is kept to a minimum. However, care is needed when using this method as topographical sources for flow disturbances outside the narrow band of terrain that is being assessed will be taken into account. Use of the DO method, discussed earlier in this paper, to gain quantitative ABL flow disruption results for a particular source are not possible due to the inadequacies of upwind fetch models over complex terrain. Comparison with a complex numerical model will provide an insight into the ability of current models to predict flow differences. Finally, the results in this paper may link to recent studies dealing with radar observations of insects in the boundary layer (Wood *et al*., 2009; Rennie *et al*., 2010). Further work is needed to establish such a link.

6. Conclusions

The design of a simple set of equations into a model that adequately highlights areas of flow difference within an easy to read plot has been achieved. A simple laminar flow PPI model (MPPI) has been used to distinguish turbulent structures in field derived PPI scans taken during the CSIP field campaign. The MPPI was first compared to the published work of Wood and Brown (1986) using an idealized data input, before being initialized with measurements taken by the Salford Doppler lidar. By highlighting the differences between the MPPI and PPI plots, a new technique has been developed that can identify turbulent flow structures in the ABL. The difference model lidar plots have been qualitatively described with respect to potential topographic sources, by overlaying the DML on a terrain map. Although links can be seen, the DO method is difficult to describe quantitatively due to the two dimensional nature of the plot. The inability of current upwind fetch models to calculate a source for the turbulent structures over complex terrain does not allow

their potential use over this heterogeneous topography. Although the DO method showed a strong link between orography and generated flow perturbation, no such link was found between these structures and smaller scale roughness elements with an aerodynamic roughness length of less than 0.3.

A method of reducing the DMLs into a one dimensional state was devised, allowing a more quantitative approach to describing the effect of orography on the ABL. Differences along the mean wind direction overlay an orographic cross section for each scan. CSD was used to assess the impact of major topographic features on the ABL by assigning a maximum difference in flow speed to each. Several assumptions need to be taken into account when using the CSD method, the major one being the inability to account for topography outside the one dimensional data set. As the topography of complex terrain is unique to a location, it is important to note that the results of this paper are site specific. The technique, however, can be applied to any number of locations and at a variety of scales, dependent on the specification of the instrumentation used.

Results have been compared to both simple and complex ABL flow prediction models. The CSD data are contrasted with a very simple one dimensional orographic model, while the DMLs are directly compared with the much more complex weather research and forecasting (WRF) model. These comparisons are to be discussed further in a subsequent paper.

Acknowledgement

This work was part of that carried out for a PhD submission supported by the Natural Environment Research Council CSIP programme.

Appendix: List of Acronyms.

ABL – Atmospheric Boundary Layer
AWS – Automatic Weather Station
CSD – cross section DML
CSIP – Convective Storm Initiation Project
DO – DML overlay
Down days – non-IOP days
DML – Difference Model Lidar plot
IOP – Intense Observation Period
LES – Large Eddy Simulation
MPPI – Modelled output PPI
NWP – Numerical Weather Prediction
PPI – Plan Position Indicator
SNR – Signal to Noise Ratio
VAD – Velocity Azimuth Display
WRF – Weather Research and Forecasting numerical model
Z_o – roughness length

References

Barkwith A. 2009. Observation and modelling of variability in flow over complex terrain, PhD thesis, School of Environmental and Life Sciences, University of Salford, Salford, United Kingdom.

Bradley EF. 1980. An experimental study of the profiles of wind speed, shearing stress and turbulence at the crest of a large hill. *Quarterly Journal of the Royal Meteorological Society* **106**: 101–124.

Browning KA, Wexler R. 1968. The determination of kinematic properties of a wind field using Doppler radar. *Journal of Applied Meteorology* **7**: 105–113.

Browning KA, Blyth AM, Clark PA, Corsmeier U, Morcrette CJ, Agnew JL, Ballard SP, Bamber D, Barthlott C, Bennett LJ, Beswick KM, Bitter M, Bozier KE, Brooks BJ, Collier CG, Davies F, Deny B, Dixon MA, Feuerle T, Forbes RM, Gaffard C, Gray MD, Hankers R, Hewison TJ, Kalthoff N, Khodayer S, Kohler M, Kottmeier C, Kraut S, Kunz M, Ladd DN, Lean HW, Lenfant J, Zhihong L, Marsham J, McGregor J, Mobbs SD, Nicol J, Norton E, Parker DJ, Perry F, Ramatschi M, Ricketts HMA, Roberts NM, Russell A, Schulz H, Slack EC, Vaughan G, Waigt J, Watson RJ, Webb AR, Wareing DP, Wieser A. 2007. The convective storm initiation project. *Bulletin of the American Meteorological Society* **88**: 1939–1955.

Coppin PA, Bradley EF, Finnigan FF. 1994. Measurements of flow over an elongated ridge and its thermal stability dependence: the mean field. *Boundary Layer Meteorology* **69**: 173–199.

Davies F, Collier CG, Bozier KE, Pearson GN, Vosper S. 2001. On the accuracy of retrieved wind information from Doppler lidar observations of flow over the Malvern hills. *Quarterly Journal Royal Meteorological Society* **129**: 321–334.

Deardorff JW. 1970. Preliminary results from numerical integrations of the unstable planetary boundary layer. *Journal of the Atmospheric Science* **27**: 1209–1211.

Finnigan JJ, Neil D, Lees BG, Croome RJ, Woodgate M. 1990. Modelling the wind flow pattern around a parabolic sand dune. *Mathematics and Computers in Simulation* **32**(1–2): 89–94.

Founda D, Tombrou M, Lalas DP, Asimakopoulos DN. 1997. Some measurements of turbulence characteristics over complex terrain. *Boundary Layer Meteorology* **83**: 221–245.

Jackson PS, Hunt JCR. 1975. Turbulent wind flow over a low hill. *Quarterly Journal of the Royal Meteorological Society* **101**: 929–955.

Mason PJ. 1994. Large eddy simulation: a critical review of the technique. *Quarterly Journal of the Royal Meteorological Society* **120**: 1–26.

Pearson GN, Collier CG. 1999. A pulsed coherent C02 lidar for atmospheric monitoring. *Quarterly Journal of the Royal Meteorological Society* **125**: 2703–2721.

Reid S. 2003. Hilltop wind profiles using SODAR. *Boundary Layer Meteorology* **108**: 315–314.

Rennie SJ, Illingworth AJ, Dance SL, Ballard SP. 2010. The accuracy of Doppler radar wind retrievals using insects as targets. *Meteorological Applications* **17**: 419–432.

Rose T, Czekala H. 2008. *RPG's Atmospheric Remote Sensing Radiometers: User Manual*. Radiometer Physics GmbH: Meckenheim, Germany.

Schmid HP. 1994. Source areas for scalars and scalar fluxes. *Boundary Layer Meteorology* **67**: 293–318.

SEE. 2008. CSIP 2005 Field Catalogue. http://www.see.leeds.ac.uk/research/ias/clouds/current/csip/operations_summary.html/. (Accessed 17 October 2008).

Walmsley JL, Taylor PA, Keith T. 1986. A simple model of neutrally stratified boundary-layer flow over complex terrain with surface roughness modulations. *Boundary Layer Meteorology* **52**: 157–186.

Wood VT, Brown RA. 1986. Single Doppler velocity signature interpretation of non-divergent environmental winds. *Journal of the Atmospheric Ocean Technology* **3**: 114–128.

Wood N, Mason PJ. 1993. The pressure force induced by neutral, turbulent flow over hills. *Quarterly Journal of the Royal Meteorological Society* **119**: 1233–1267.

Wood CR, O'Connor EJ, Hurley RA, Reynolds DR, Illingworth AJ. 2009. Cloud-radar observations of insects in the UK convective boundary layer. *Meteorological Applications* **16**: 491–500.

Wyngaard JC. 2010. *Turbulence in the Atmosphere*. Cambridge University Press: Cambridge, UK; 393.

